Vector field path following and obstacle avoidance singularity mitigation via look-ahead flight envelope

First A. Author[*] and Second B. Author Jr.[†]
Business or Academic Affiliation 1, City, State, Zip Code

Unmanned Aerial Vehicles conventionally navigate by following a series of pre-planned waypoints that may have to be re-planned when flying in a dynamic environment or encountering previously unknown obstacles. Waypoints are generally planned off-line and relayed to the UAV, taking up time and autopilot communication resources. Attractive path following and repulsive obstacle avoidance vector fields have been summed together to produce UAV guidance that follows pre-planned paths and avoids obstacles without the need to re-plan. Summing attractive and repulsive vector fields may produce small regions of null guidance, called singularities, which could potentially lead to trap situations. An investigation into singularity mitigation by vector field weight parameterization is presented.

I. Nomenclature

UAV	=	Unmanned Aerial Vehicle
VF	=	Vector Field
VFF	=	Virtual Force Field
LVF	=	Lyapunov Vector Field
GVF	=	Goncalves Vector Field
$\overrightarrow{X}$	=	UAV position
$\overrightarrow{U}$	=	UAV velocity
θ	=	UAV heading
$\dot{\theta}$	=	UAV heading rate
u	=	UAV speed
dt	=	discrete time step
$\overrightarrow{V}_{conv}$	=	Convergence Vector
$\overrightarrow{V}_{circ}$	=	Circulation Vector
G	=	Convergence Weight
H	=	Circulation Weight
V	=	Potential Function
r_O	=	Obstacle Radius
R	=	Decay Radius
γ	=	Path Deviation Cost
α_i	=	Surface Function
x	=	UAV horizontal position
y	=	UAV vertical position
x_c	=	Circular obstacle horizontal position
y_c	=	Circular obstacle vertical position
d	=	Range to obstacle
P	=	Obstacle Decay Weight

[*]Insert Job Title, Department Name, Address/Mail Stop, and AIAA Member Grade (if any) for first author.
[†]Insert Job Title, Department Name, Address/Mail Stop, and AIAA Member Grade (if any) for second author.

II. Introduction

Unmanned Aerial Vehicles (UAV)s are pilotless aircraft used by military, police, and civilian communities for tasks such as reconnaissance, damage assessment, surveying, and target tracking [1, 2]. Many of these tasks depend on the UAVs ability to autonomously follow a pre-planned path while manually avoiding obstacles. Pre-planned paths are typically generated on a remote ground station and relayed to the UAV's autopilot. On-board guidance systems attempt to minimize the lateral error to the path by commanding a heading pointing to the path. Guidance methods for following a pre-planned path include geometric methods such as waypoint or carrot chasing and control techniques such as proportional-integral-derivative (PID), non-linear guidance laws, and linear quadratic regulator (LQR) [17]. Due to traditional guidance method's dependence on a path planner to construct an obstacle free and flyable path, these methods often lack a mechanism to avoid new obstacles. Re-planning and relaying a new obstacle free path may be impossible under certain conditions, such as flying beyond line-of-sight. Path planning on-board to avoid a new obstacle could be accomplished by inserting a new temporary path or by completely re-planning, however introduces several challenges such as waypoint placement and density.

Additional methods for avoiding obstacles in real time include potential field [9, 10] and vector field [21, 23–26] which employ the use of artificial attractive and repulsive forces to pull a UAV towards a goal while pushing away from nearby obstacles. Potential field has been used as a path planner and guidance system in obstacle rich environments, however suffers from several limitations including local minima, oscillations, and may cause excess deviation from the desired path. Vector field guidance (VFG) converges and circulates a pre-defined path and may be summed with additional repulsive vector fields to produce an obstacle avoidance. Each field's behavior can be modified by weighting convergence, circulation, and time-varying components by multiplicative scalars. Previous investigations into vector field obstacle avoidance only considered negative static weights for convergence which did not aid in circumnavigating an obstacle and can introduce conditions which lead to guidance singularities.

Further optimization of vector fields to include circulation can produce a real-time guidance for circumnavigating obstacles that lie along a pre-planned path while also removing singularities from the UAVs route. A method for determining obstacle decay radius, circulation, and repulsion such that a UAV avoids obstacles while minimizing deviation from the planned path is presented. The modified guidance will then be compared against waypoint, Potential Field, and un-modified path following guidance in simulation for cross track error from planned path.

III. Literature

The dynamics of UAVs are often simplified when simulating guidance systems by modeling the UAV as a Dubin's vehicle [18–21, 23]. It is assumed that the autopilots control system is capable of maintaining stability, speed u, and can turn the vehicle at a fixed turn rate $\dot{\theta}$. The position of the UAV $\overrightarrow{X}$ at time t is calculated from the integral of the velocity vector $\overrightarrow{U}$, Equation 2. Heading is an input from a guidance system, such as waypoint, potential field, or vector field.

$$\overrightarrow{U}(t) = u \begin{bmatrix} cos(\theta(t)) \\ sin(\theta(t)) \end{bmatrix} \tag{1}$$

$$\overrightarrow{X}(t) = \overrightarrow{U}dt + \overrightarrow{X}(t-1) \tag{2}$$

$$\dot{\theta} \leq 20deg/s \tag{3}$$

Waypoint guidance aligns the vehicle with the current active waypoint that lies along a pre-planned path. Paths are typically generated off-line and can be optimized for shortest distance traveled and further refined to be flyable for a particular vehicle. Paths may also be optimized to produce flight patterns that increase sensor coverage of an area of interest [6].

If an obstacle lies along that sensor path, the UAV must avoid the obstacle but also return back to the sensor path such that a minimal length of the path is missed during data collection. The number of waypoints that divert around an obstacle effects how closely the UAV tracks the outside of the obstacle and how much of the original path can be traveled. Few obstacle diversion waypoints leads to excess path deviation. Increasing the number of diversion waypoints reduces path deviation, however has diminishing returns. A cost function γ can be used to measure the deviation from a planned path while avoiding obstacles with diversion waypoints, shown in Equation 4.

$$\gamma = \frac{1}{r_O} \int_0^{tf} y dt \tag{4}$$

An example of a UAV following diversion waypoints is shown in Figure 1 and the cost associated with increasing number of waypoints in Figure 2.

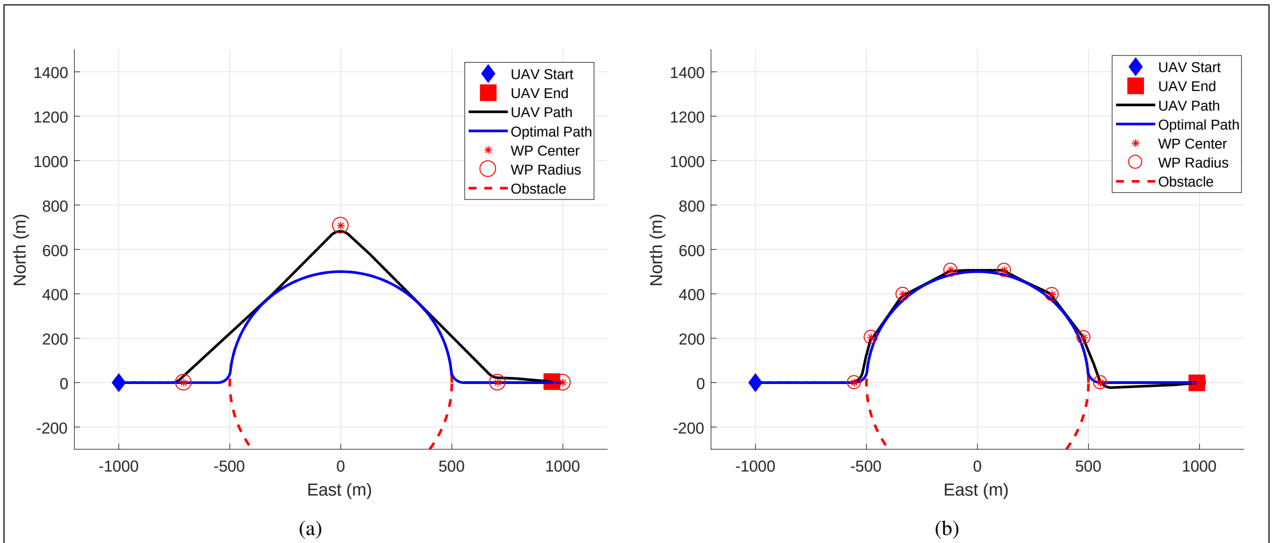

Fig. 1 Obstacle Diversion Waypoints

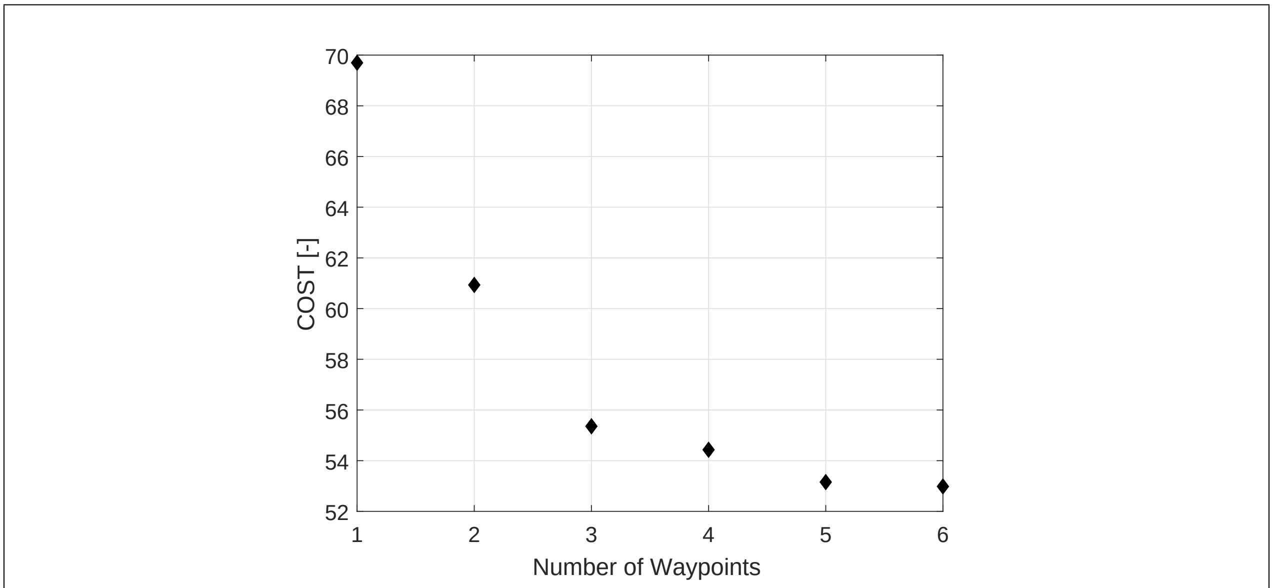

Fig. 2 Cost impact versus number of waypoints

It would be beneficial to include obstacle avoidance into a UAVs guidance system to remove the need to communicate with the ground station or use an on-board path planner which may be accomplished with potential field or vector field.

Potential field is based on the principle of artificial attractive and repulsive forces acting on a point mass to guide a system to a desired goal while avoiding static and dynamic obstacles [7]. Goals are represented as an attractive force that pull a point mass in the direction of minimal energy while obstacles are represented as repulsive forces that act locally to push the point mass away. Potential field is also capable of acting as a path and trajectory planning algorithm [8], possibly eliminating the off-board path planner. An example of potential field can be found in [9–11] which allowed for real time goal seeking with obstacle avoidance on a mobile ground robot equipped with ultrasonic sensors. The robot was attracted towards a goal with constant magnitude force. In the immediate area of the robot, an active window exists which records integer certainty values inside discrete cells. Cells containing an obstacle provide a repulsive force opposite in direction to the line-of-sight from vehicle to cell location. The total repulsive force exerted on the robot is determined by summing the active cells. Summing together attractive and repulsive forces produce a vector that can be used for heading guidance.

Major drawbacks to potential field were identified in [11] consisting of local minimum and oscillations in corridors. The local minimum problem occurs when closely spaced obstacle's potential combine to produce a well on the descent gradient where a pre-mature stable point is reached. Proposed solutions to local minimum include object clustering and virtual waypoint method [12], virtual escaping route [13], and use of navigation functions [14]. Oscillations in potential field were addressed in [15] and [16]. In addition to local minimum and oscillations, potential field may not be ideal for providing guidance to return to a sensor path after avoiding an obstacle. Once the obstacle has been avoided, the attractive goal will direct the UAV in a straight path which may not lie along the sensor line. Guidance that follows an explicit path, deviates when necessary to avoid obstacles, and return back to the explicit path quickly can be accomplished with path following vector fields.

Vector fields produce continuous heading guidance that asymptotically converges and circulates a path. A comparison between vector field and waypoint guidance techniques was presented in [17] where each method was evaluated based on its complexity, robustness, and accuracy. The vector field model produced guidance that was both robust to external wind disturbances while maintaining a low cross track error. The two most prominent methods for generating vector fields in literature consist of the Lyapunov Vector Field (LVF) [18–23] and Gradient Vector Field (GVF) [24–27] method. LVFs for converging and following straight and circular paths were described in [18]. Straight and circular path vector fields can be selectively activated throughout flight to form more complex paths, shown in [18–20, 28]. LVF for curved path following was presented in [23] which may allow for more complex paths and eliminates the need to switch between vector fields.

The Gradient Vector Field (GVF) method produces a similar field to LVF, however has several advantages over LVFs. GVF produces an n-dimensional vector field that converges and circulates to both static and time varying paths, which may be useful for tracking dynamic paths or avoiding dynamic obstacles. Additionally, convergence, circulation, and time-varying terms that make up the GVF are decoupled from each other allowing for easy weighting of the total field. GVFs converge and circulate at the intersection, or level set, of $n-1$ dimensional implicit surfaces $(\alpha_i : \mathbb{R}^n \rightarrow \mathbb{R} | i = 1, ..., n-1)$. The integral lines of the field are guaranteed to converge and circulate the level set when two conditions are met: 1) the implicit surface functions are positive definite and 2) have bounded derivatives.

The total vector field for a static path $\overrightarrow{V}$ is calculated by:

$$\overrightarrow{V} = G\nabla V + H \wedge_{i=1}^{n-1} \nabla\alpha_i \tag{5}$$

or in component form:

$$\overrightarrow{V} = G\overrightarrow{V}_{conv} + H\overrightarrow{V}_{circ} \tag{6}$$

where $\overrightarrow{V}_{conv}$ produces vectors perpendicular to the path and $\overrightarrow{V}_{circ}$ produces vectors parallel to the path. The multiplicative factors G, H, and L are scalar weights to influence the strength of each field component.

Convergence is calculated by:

$$\overrightarrow{V}_{conv} = \nabla V \tag{7}$$

where the potential function V is:

$$V = -\sqrt{{\alpha_1}^2 + {\alpha_2}^2} \tag{8}$$

$$\nabla V = \begin{bmatrix} \frac{dV}{dx} \\ \frac{dV}{dy} \\ \frac{dV}{dz} \end{bmatrix} \tag{9}$$

Circulation is calculated by taking the wedge product of the gradients of the surface functions:

$$\overrightarrow{V}_{circ} = \wedge_{i=1}^{n-1} \nabla\alpha_i \tag{10}$$

In the case of ($n = 3$) the wedge product simplifies as the cross product:

$$\overrightarrow{V}_{circ} = \nabla\alpha_1 \times \nabla\alpha_2 \tag{11}$$

Intersecting two flat planes ($\alpha_1 = z, \alpha_2 = x$) produces a GVF that converges and circulates a straight path.

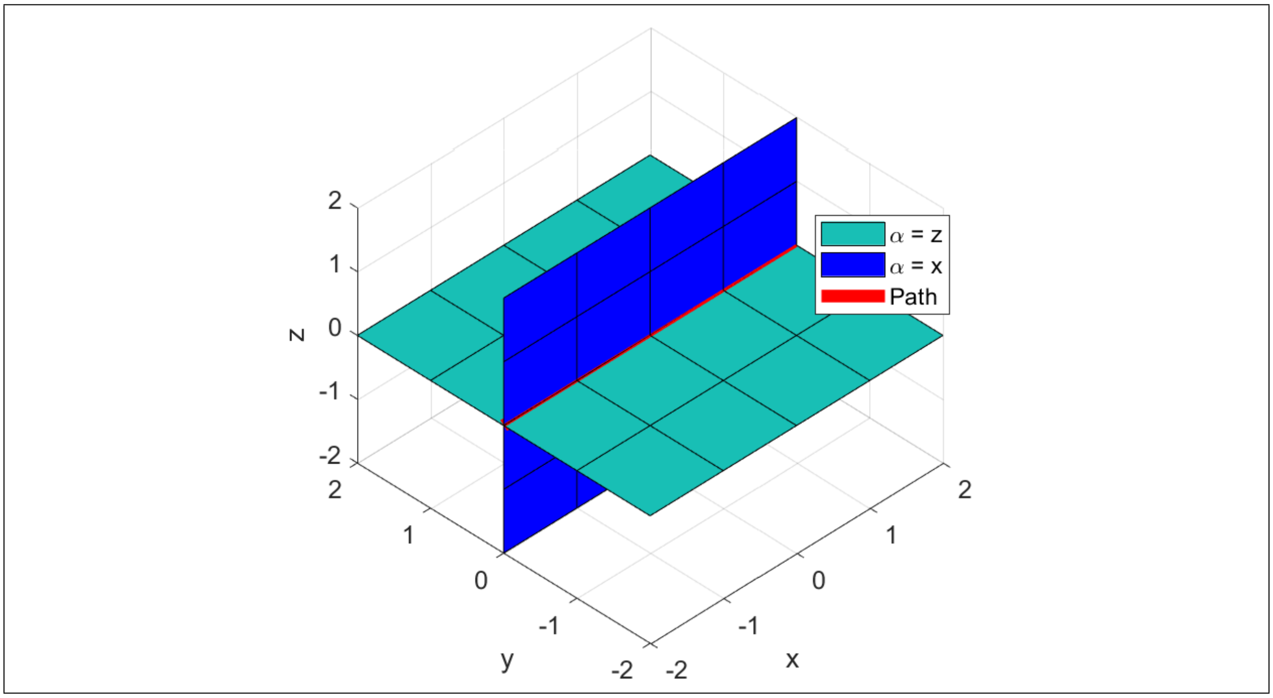

Fig. 3 Plane intersection

How quickly the path following field transitions from convergence to circulation depends on the field weights. Equal parts convergence and circulation are shown in Figure 4a ($G = H = 1$) and a larger circulation value in Figure 4b ($G = 1, H = 5$).

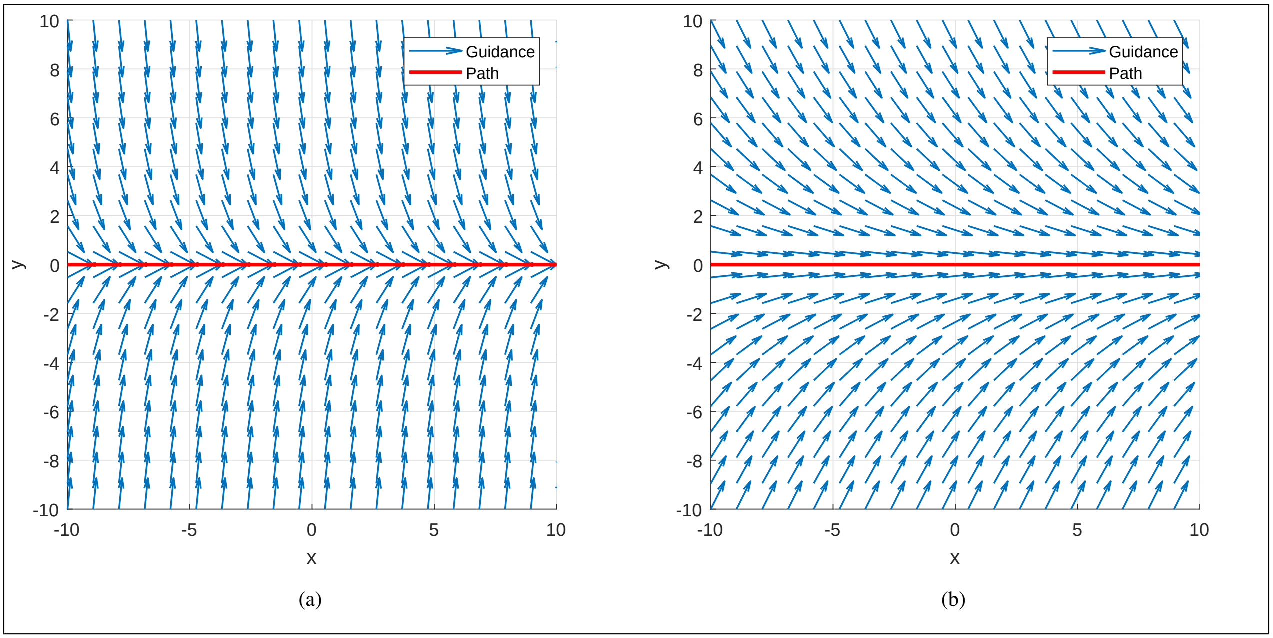

Fig. 4 GVF converging and a) small circulation b) large circulation

GVF was compared against LVF in a standoff tracking scenario in [Wilhelm] where a fixed wing UAV was tasked with with loitering around a moving ground target while avoiding static obstacles. A circular time-varying attractive vector field was attached to a moving ground target. Static circular repulsive vector fields centered at the obstacles and weighted by hyperbolic tangent decay functions were summed with the attractive circular field to produce a target loitering and obstacle avoidance guidance. The performance of Lyapunov [21] and gradient vector field [24–26] were compared for their cross track error with respect to the loiter circle. Gradient vector field had favorable performance due to compensation for a time-varying vector field. The gradient vector field technique also has the benefit of decoupled weighting parameters for convergence, circulation, and time-varying terms, allowing for easy modification of field behavior.

The presence of singularities were not addressed in [Wilhelm], mentioned briefly in [18] and observed in [29]. For fixed wing UAVs the lack of guidance may prevent the UAV from avoiding an obstacle, while multi-rotor UAVs may end up in a trap situation. Singularities may be present at any location where a goal field and obstacle field are of equal strength. Detecting singularities and modifying the GVF for an improved obstacle avoidance is now considered.

IV. Methods

The static weight vector field for straight lines and circular obstacles will be presented. A numerical method for detecting singularities in a summed vector field will be discussed. The modified vector field law with dynamic weights will be presented. Simulations comparing waypoint, potential field, and vector field guidance will be presented for worst case scenario with an obstacle centered on the sensor path.

A. Path Following with GVF

Path following guidance for a planar UAV at position (x, y) for a time invariant line is achieved by summing together convergence $\overrightarrow{V}_{conv}$ and circulation $\overrightarrow{V}_{circ}$ terms shown in Equation 6, where the plane defined by implicit surface function α_1 is at angle δ and plane α_2 is at constant height of $Z = 1$ shown in Equations 12 and 13 respectively.

$$\alpha_1 = cos(\delta)x + sin(\delta)y \tag{12}$$

$$\alpha_2 = z \tag{13}$$

The gradient potential, ∇V is shown in Equation 14.

$$\nabla V = -\frac{1}{2(\sqrt{\cos^2(\delta)x^2 + 2\cos(\delta)\sin(\delta)xy + \sin^2(\delta)y^2})} \begin{bmatrix} 2x\cos^2(\delta) + 2\cos(\delta)\sin(\delta)y \\ 2y\sin^2(\delta) + 2\cos(\delta)\sin(\delta)x \\ 2 \end{bmatrix} \tag{14}$$

Circulation is calculated by the cross product of the surface function gradients, which evaluates to that shown in Equation 15.

$$\overrightarrow{V}_{circ} = \begin{bmatrix} sin(\theta) \\ -cos(\theta) \\ 0 \end{bmatrix} \tag{15}$$

Guidance for a path at angle $\delta = 0$ and equal parts circulation and convergence weights $G = H = 1$ is shown in Figure 4a.

B. Avoidance

A circular avoidance vector field centered at (x_c, y_c) is constructed by intersecting a cylinder, Equation 16, and a plane 13.

$$\alpha_1 = (x - x_c)^2 + (y - y_c)^2 - r^2 \tag{16}$$

Convergence is calculated by the gradient of the potential function 14, which when simplified evaluates to

$$\nabla V = A\overrightarrow{B} \tag{17}$$

where

$$A = \frac{-1}{\sqrt{\bar{x}^4 + \bar{y}^4 + 2\bar{x}^2\bar{y}^2 - 2r^2\bar{x}^2 - 2r^2\bar{y}^2 + r^2 + z^2}} \tag{18}$$

$$\overrightarrow{B} = \begin{bmatrix} 2\bar{x}^3 + 2\bar{x}\bar{y}^2 - 2r^2\bar{x} \\ 2\bar{y}^3 + 2\bar{x}^2\bar{y} - 2r^2\bar{y} \\ z \end{bmatrix} \tag{19}$$

and

$$\bar{x} = x - x_c \tag{20}$$

$$\bar{y} = y - y_c \tag{21}$$

Circulation is calculated from the cross product of each implicit surface function's gradient, which simplifies to

$$\overrightarrow{V}_{circ} = \begin{bmatrix} 2(y - y_c) \\ -2(x - x_c) \\ 0 \end{bmatrix} \tag{22}$$

Strictly repulsion guidance is produced by assigning a negative weight to the convergence term $G = -1$, no circulation $H = 0$, and a small path radius r to prevent trap situations. Limiting the distance at which the field has influence is achieved with a decay function shown in Equation 23 where d is the range to the center of the obstacle and R is the radius where the field has near zero strength.

$$P = -\tanh\left(\frac{2\pi d}{R} - \pi\right) + 1 \tag{23}$$

$$d = \sqrt{\bar{x}^2 + \bar{y}^2} \tag{24}$$

A strictly repulsive field $\overrightarrow{V}_{obst}$ with $G = -1$, $H = 0$, $r = 0.01$, and $R = 35$ is shown in Figure 5a. Adding equal magnitude circulation and decay $G = -1$, $H = 1$ is shown in Figure 5b.

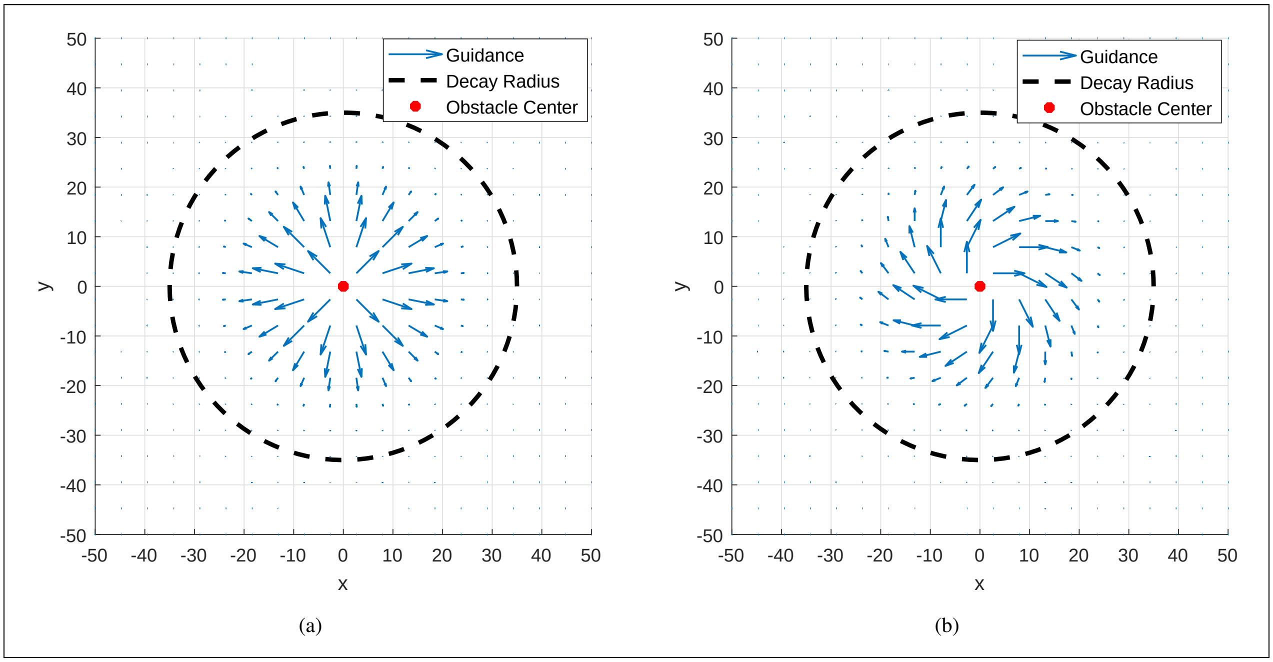

Fig. 5 Repulsive GVF a) no circulation and b) with circulation

Path following guidance and repulsive obstacle avoidance is achieved by summing the two fields together, producing the UAVs guidance $\overrightarrow{V}_G$ shown in Equation 25

$$\overrightarrow{V}_g = \overrightarrow{V}_{path} + P\overrightarrow{V}_{obst} \tag{25}$$

Singularities may be present in the above guidance due to the repulsive vectors of the obstacle canceling out the path following vectors. Identifying the location of these singularities will now be addressed.

C. Singularity Detection

Singularities are expected to exist where the magnitude of the vector $\overrightarrow{V}_g$ has a magnitude equal to zero, shown in Equation 26. An analytical solution to Equation 26 may be difficult to obtain, therefore a numerical approach with initial conditions placed at the radius of equal strength, $R/2$, can be used.

$$||\overrightarrow{V}_g|| = 0 \tag{26}$$

D. Static Modified Weights

Determining the decay radius R and circulation weight H for a repulsive vector field depends on the UAVs speed u and turnrate $\dot{\theta}$. An obstacle located at a lateral distance Y_0 from the pre-planned sensor path has a radius r_O equal to a scalar multiple of the UAVs turn radius, shown in Equation 27. The multiple n is bounded on the interval $[1, \infty)$.

$$r_O = n\theta_r \tag{27}$$

The repulsive field decay radius R, expressed in k multiples of the obstacles radius is shown in Equation 28 and also bounded on the interval $[1, \infty)$.

$$R = kr_O \tag{28}$$

The decay multiple k and circulation H are then determined by minimizing the cost function 29, where y is the lateral deviation from the path in the I frame and the function j penalizes the UAV for entering the obstacle radius. The sign of H can be determined from the LOS angle between the UAV and the obstacle such that the UAV travels around the obstacle in the correct, least distance, direction.

$$\underset{H,k}{\text{minimize}} \quad \frac{1}{R}\int_{t_f}^{0} y dt + j(x, y) \tag{29}$$

$$j(x, y) = \begin{cases} 100dt & \sqrt{(x-xc)^2 + (y-yc)^2} \leq r_O \\ 0 & \sqrt{(x-xc)^2 + (y-yc)^2} > r_O \end{cases} \tag{30}$$

A comparison of a UAVs route using a strictly repulsive vector field versus a vector field with circulation is shown in Figure 6. A UAV with a speed of $u = 20m/s$ and turning rate of $\dot{\theta} = 20deg/s$ following a straight vector field path is shown avoiding an obstacle of radius $n = 2$.

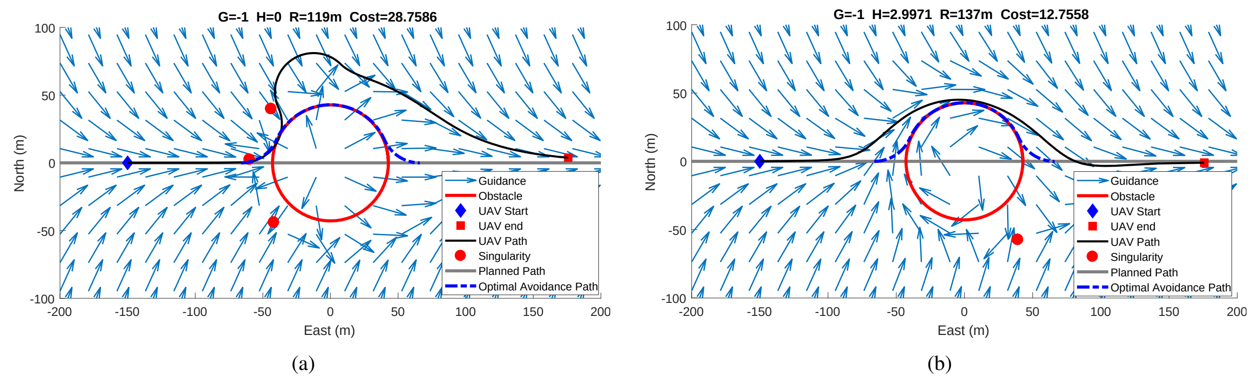

Fig. 6 Repulsive and Circulating VF Guidance UAV Route

The definition of obstacle and decay field radius in terms of vehicle turn radius θ_r allows for a single decay factor k and circulation H to be applicable for multiple velocities. This generalizes the avoidance field parameter selection problem and allows for a two dimensional lookup table to be generated for a number of obstacle radius factors n and obstacle lateral positions Y_0 for real time obstacle avoidance.

E. Optimal Avoidance Route for Straight Path

A geometrically optimal route around a circular obstacle can be used to compare the performance of avoidance algorithms. The path for avoiding a circular obstacle while maximizing the sensor path coverage can be accomplished with three circular arc turns. The circular obstacle is defined to have a radius R and a lateral distance Y_0 from the sensor path in frame I. The first and third arc utilize the UAVs minimum turning radius, θ_r, calculated in Equation 31. The start of the first minimum radius turn begins when the UAV's horizontal position x reaches $\tilde{x}$ from the path frame origin. At a horizontal position $-\hat{x}$ the UAV turns with a radius of the obstacle R and exits when the UAVs horizontal position reaches $\hat{x}$.

$$\theta_r = \frac{u}{\dot{\theta}} \tag{31}$$

The horizontal points $\tilde{x}$ and $\hat{x}$ are shown in Equations 32 and 33 respectively.

$$\widetilde{x} = -\sqrt{(\theta_r + R)^2 - (\theta_r - Y_o)^2} \tag{32}$$

$$\hat{x} = \frac{R\sqrt{(r + R)^2 - (\theta_r - Y_o)^2}}{R + \theta_r} \tag{33}$$

The avoidance path for navigating around a circular obstacle with maximum coverage of a sensor line is defined in Equation 34 and shown in Figure 7.

$$y(x) = \begin{cases} \widetilde{y} - \sqrt{\theta_r^2 - (x - \widetilde{x})^2} & x < -\hat{x} \\ Y_o + \sqrt{R^2 - x^2} & -\hat{x} \le x \ge \hat{x} \\ \widetilde{y} - \sqrt{\theta_r^2 - (x + \widetilde{x})^2} & x > -\hat{x} \end{cases} \tag{34}$$

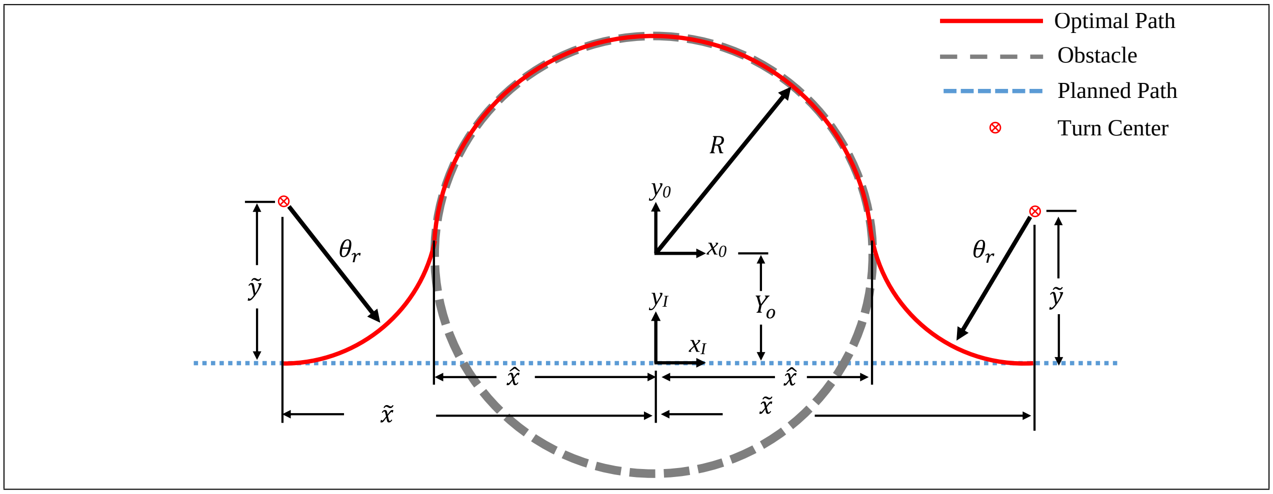

Fig. 7 Optimal Kinematic Path Around Circular Obstacle

The avoidance path represents the optimal path around a circular obstacle and would be used to generate waypoints for waypoint guidance.

V. Simulations

A comparision of waypoint, VFF, strictly repulsive GVF, and the modified weighted GVF were compared for both their deviation from the sensor path and how closely the avoidance followed an optimal path around the obstacle. For each guidance method, the UAV is tasked with following a straight sensor path. An obstacle located at $(0, 0)$ must be avoided. Waypoints were generated around the obstacle using the optimal avoidance path with a waypoint radius of 20 meters. The VFF provided a attractive force for the goal of 0.8 while the obstacle provided a repulsive force of -2. With an obstacle width of 5 meters and field exponential of $n = 2$, the VFF avoids the obstacle and gradually returns to the path.

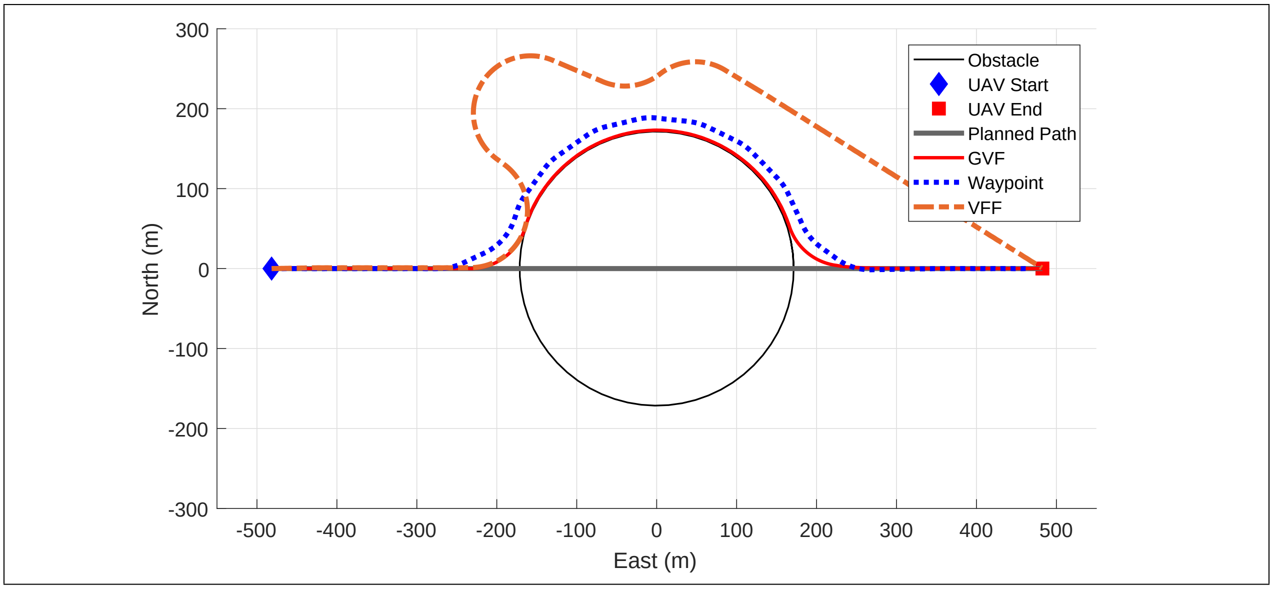

Fig. 8 Path of UAV guided by guidance methods

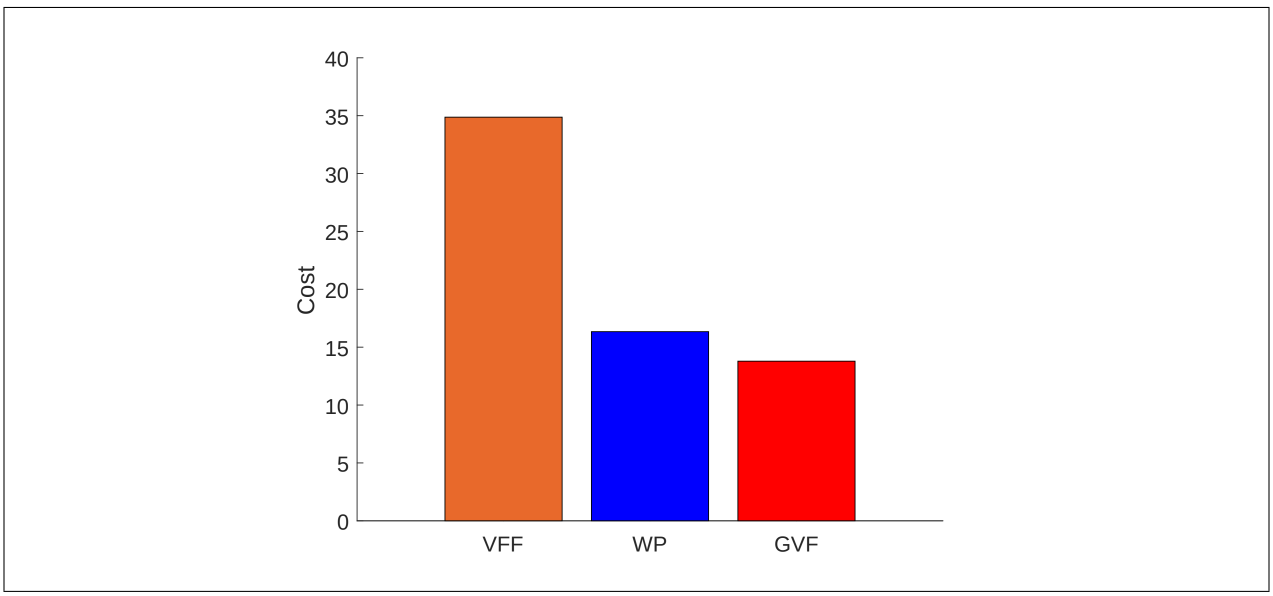

Fig. 9 Cost performance for various UAV guidance methods

VI. Conclusion

Vector field guidance with optimized weights for avoiding obstacles and minimally deviating from a planned path was presented and compared to guidance methods in literature. Conventional methods for avoiding obstacles may require human intervention and require paths to be re-planned, such as waypoint navigation. Potential field eliminates the need for a path planner when encountering a new obstacle, however is not ideal for path following scenarios such as surveying a sensor line. Vector field guidance avoids re-planning and avoids an obstacle while returning to the original pre-planned path by selecting decay radius and circulation that minimizes a path deviation cost function. Singularities in the vector field are also avoided when circulation is added to the decay field. Future work to improve vector field for avoidance may include optimizing field parameters at each time step, potentially increasing time spent on the sensor line.

References

[1] Ariyur, K. B., and Fregene, K. O., "Autonomous tracking of a ground vehicle by a UAV," *American Control Conference, 2008*, IEEE, 2008, pp. 669–671.

[2] Teuliere, C., Eck, L., and Marchand, E., "Chasing a moving target from a flying UAV," *Intelligent Robots and Systems (IROS), 2011 IEEE/RSJ International Conference on*, IEEE, 2011, pp. 4929–4934.

[3] Oh, H., Kim, S., Shin, H.-S., Tsourdos, A., and White, B., "Coordinated standoff tracking of groups of moving targets using multiple UAVs," *Control & Automation (MED), 2013 21st Mediterranean Conference on*, IEEE, 2013, pp. 969–977. URL `http://ieeexplore.ieee.org/abstract/document/6608839/`.

[4] Hyondong Oh, Seungkeun Kim, Hyo-sang Shin, and Tsourdos, A., "Coordinated standoff tracking of moving target groups using multiple UAVs," *IEEE Transactions on Aerospace and Electronic Systems*, Vol. 51, No. 2, 2015, pp. 1501–1514. doi:10.1109/TAES.2015.140044, URL `http://ieeexplore.ieee.org/document/7126199/`.

[5] Ulun, S., and Unel, M., "Coordinated motion of UGVs and a UAV," *Industrial Electronics Society, IECON 2013-39th Annual Conference of the IEEE*, IEEE, 2013, pp. 4079–4084. URL `http://ieeexplore.ieee.org/abstract/document/6699789/`.

[6] Wilhelm, J., Clem, G., and Eberhart, G., "Direct Entry Minimal Path UAV Loitering Path Planning," *Aerospace*, Vol. 4, No. 2, 2017, p. 23. doi:10.3390/aerospace4020023, URL `http://www.mdpi.com/2226-4310/4/2/23`.

[7] Khatib, O., "Real-time obstacle avoidance for manipulators and mobile robots," *The international journal of robotics research*, Vol. 5, No. 1, 1986, pp. 90–98. URL `http://journals.sagepub.com/doi/abs/10.1177/027836498600500106`.

[8] Rimon, E., "Exact Robot Navigation Using Artificial Potential Functions.pdf," , 1992.

[9] Borenstein, J., and Koren, Y., "Real-time obstacle avoidance for fast mobile robots in cluttered environments," *Robotics and Automation, 1990. Proceedings., 1990 IEEE International Conference on*, IEEE, 1990, pp. 572–577. URL `http://ieeexplore.ieee.org/abstract/document/126042/`.

[10] Borenstein, J., and Koren, Y., "The vector field histogram-fast obstacle avoidance for mobile robots," *IEEE transactions on robotics and automation*, Vol. 7, No. 3, 1991, pp. 278–288. URL `http://ieeexplore.ieee.org/abstract/document/88137/`.

[11] Koren, Y., and Borenstein, J., "Potential Field Methods and their inherent limitions for morbile robot navigation.pdf," , 1991. URL `http://ieeexplore.ieee.org/document/131810/`.

[12] Liu, Y., and Zhao, Y., "A virtual-waypoint based artificial potential field method for UAV path planning," *Guidance, Navigation and Control Conference (CGNCC), 2016 IEEE Chinese*, IEEE, 2016, pp. 949–953. URL `http://ieeexplore.ieee.org/abstract/document/7828913/`.

[13] Kim, D. H., "Escaping route method for a trap situation in local path planning," *International Journal of Control, Automation and Systems*, Vol. 7, No. 3, 2009, pp. 495–500. doi:10.1007/s12555-009-0320-7, URL `http://link.springer.com/10.1007/s12555-009-0320-7`.

[14] Goerzen, C., Kong, Z., and Mettler, B., "A Survey of Motion Planning Algorithms from the Perspective of Autonomous UAV Guidance," *Journal of Intelligent and Robotic Systems*, Vol. 57, No. 1-4, 2010, pp. 65–100. doi:10.1007/s10846-009-9383-1, URL `http://link.springer.com/10.1007/s10846-009-9383-1`.

[15] Lei Tang, Songyi Dian, Gangxu Gu, Kunli Zhou, Suihe Wang, and Xinghuan Feng, "A novel potential field method for obstacle avoidance and path planning of mobile robot," IEEE, 2010, pp. 633–637. doi:10.1109/ICCSIT.2010.5565069, URL `http://ieeexplore.ieee.org/document/5565069/`.

[16] Li, G., Yamashita, A., Asama, H., and Tamura, Y., "An efficient improved artificial potential field based regression search method for robot path planning," IEEE, 2012, pp. 1227–1232. doi:10.1109/ICMA.2012.6283526, URL `http://ieeexplore.ieee.org/document/6283526/`.

[17] Sujit, P., Saripalli, S., and Sousa, J. B., "Unmanned Aerial Vehicle Path Following: A Survey and Analysis of Algorithms for Fixed-Wing Unmanned Aerial Vehicless," *IEEE Control Systems*, Vol. 34, No. 1, 2014, pp. 42–59. doi:10.1109/MCS.2013.2287568, URL `http://ieeexplore.ieee.org/document/6712082/`.

[18] Nelson, D. R., "Cooperative control of miniature air vehicles," 2005. URL `http://scholarsarchive.byu.edu/etd/1095/`.

[19] Nelson, D. R., Barber, D. B., McLain, T. W., and Beard, R. W., "Vector field path following for small unmanned air vehicles," *American Control Conference, 2006*, IEEE, 2006, pp. 7–pp. URL http://ieeexplore.ieee.org/abstract/document/1657648/.

[20] Nelson, D., Barber, D., McLain, T., and Beard, R., "Vector Field Path Following for Miniature Air Vehicles," *IEEE Transactions on Robotics*, Vol. 23, No. 3, 2007, pp. 519–529. doi:10.1109/TRO.2007.898976, URL http://ieeexplore.ieee.org/document/4252175/.

[21] Frew, E. W., "Cooperative standoff tracking of uncertain moving targets using active robot networks," *Robotics and Automation, 2007 IEEE International Conference on*, IEEE, 2007, pp. 3277–3282. URL http://ieeexplore.ieee.org/abstract/document/4209596/.

[22] Miao, Z., Thakur, D., Erwin, R. S., Pierre, J., Wang, Y., and Fierro, R., "Orthogonal vector field-based control for a multi-robot system circumnavigating a moving target in 3D," *Decision and Control (CDC), 2016 IEEE 55th Conference on*, IEEE, 2016, pp. 6004–6009. URL http://ieeexplore.ieee.org/abstract/document/7799191/.

[23] Griffiths, S., "Vector Field Approach for Curved Path Following for Miniature Aerial Vehicles," American Institute of Aeronautics and Astronautics, 2006. doi:10.2514/6.2006-6467, URL http://arc.aiaa.org/doi/10.2514/6.2006-6467.

[24] Goncalves, V. M., Pimenta, L. C. A., Maia, C. A., and Pereira, G. A. S., "Artificial vector fields for robot convergence and circulation of time-varying curves in n-dimensional spaces," IEEE, 2009, pp. 2012–2017. doi:10.1109/ACC.2009.5160350, URL http://ieeexplore.ieee.org/document/5160350/.

[25] Gonçalves, V. M., Pimenta, L. C., Maia, C. A., Pereira, G. A., Dutra, B. C., Michael, N., Fink, J., and Kumar, V., "Circulation of curves using vector fields: actual robot experiments in 2D and 3D workspaces," *Robotics and Automation (ICRA), 2010 IEEE International Conference on*, IEEE, 2010, pp. 1136–1141.

[26] Gonçalves, V. M., Pimenta, L. C., Maia, C. A., Dutra, B. C., and Pereira, G. A., "Vector fields for robot navigation along time-varying curves in $ n $-dimensions," *IEEE Transactions on Robotics*, Vol. 26, No. 4, 2010, pp. 647–659. URL http://ieeexplore.ieee.org/abstract/document/5504176/.

[27] Gerlach, A. R., *Autonomous Path-Following by Approximate Inverse Dynamics and Vector Field Prediction*, University of Cincinnati, 2014. URL http://search.proquest.com/openview/432d738d856bf0a9b46acea1b1eee08f/1?pq-origsite=gscholar&cbl=18750&diss=y.

[28] Jung, W., Lim, S., Lee, D., and Bang, H., "Unmanned Aircraft Vector Field Path Following with Arrival Angle Control," *Journal of Intelligent & Robotic Systems*, Vol. 84, No. 1-4, 2016, pp. 311–325. doi:10.1007/s10846-016-0332-5, URL http://link.springer.com/10.1007/s10846-016-0332-5.

[29] Panagou, D., "Motion planning and collision avoidance using navigation vector fields," *Robotics and Automation (ICRA), 2014 IEEE International Conference on*, IEEE, 2014, pp. 2513–2518. URL http://ieeexplore.ieee.org/abstract/document/6907210/.